ApJ in press

THE NUCLEAR REDDENING CURVE FOR ACTIVE GALACTIC NUCLEI AND THE SHAPE OF THE INFRA-RED TO X-RAY SPECTRAL ENERGY DISTRIBUTION

C. MARTIN GASKELL and RENÉ W. GOOSMANN [1]

Department of Physics & Astronomy, University of Nebraska, Lincoln, NE 68588-0111

mgaskell1@unl.edu

rene.goosmann@obspm.fr

and

ROBERT R. J. ANTONUCCI and DAVID H. WHYSONG

Department of Physics & Astronomy, University of California, Santa Barbara, CA 93106

ski@spot.physics.uscb.edu

dwhysong@spot.physics.uscb.edu

ABSTRACT

We present extinction curves derived from the broad emission lines and continua of samples of 72 radio-loud and 1018 radio-quiet AGNs. The curves are significantly flatter in the UV than are curves for the local ISM. The reddening curves for the radio-quiet LBQS quasars are slightly steeper than those of the radio-loud quasars in the UV, probably because of additional reddening by dust further out in the host galaxies of the former. The UV extinction curves for the radio-loud AGNs are very flat. This is explicable with slight modifications to standard MRN dust models: there is a relative lack of small grains in the nuclear dust. Our continuum and broad-emission line reddening curves agree in both shape and amplitude, confirming that the continuum shape is indeed profoundly affected by reddening for all but the bluest AGNs. With correction by

[1]Present address: Observatoire de Paris, Section de Meudon, LUTH, Place Jules Janssen, F-92195 Meudon Cedex, France

our generic extinction curve, all of the radio-loud AGNs have continuous optical-UV spectra consistent with a single shape. We show that radio-quiet AGNs have very similar intrinsic UV to optical shape over orders of magnitude in luminosity. We also argue that radio-loud and radio-quiet AGNs probably share the same underlying continuum shape and that most of the systematic differences between their observed continuum shapes are due to higher nuclear reddening in radio-selected AGNs, and additional reddening from dust further out in the host galaxies in radio-quiet AGNs. Our conclusions have important implications for the modelling of quasar continua and the analysis of quasar demographics.

Subject headings: galaxies:active — ISM:dust, extinction - galaxies:quasars:general — X-rays:galaxies — black hole physics — accretion: accretion disk

1. INTRODUCTION

Poor characterization of the extinction in Active Galactic Nuclei (AGNs) has been one of the biggest obstacles to understanding their nature. Without knowledge of the appropriate form and amplitude of the wavelength dependence of the extinction it is impossible to determine the true spectral energy distribution (SED). It is also difficult to interpret emission-line spectra to diagnose conditions nears the black hole. There has been a long-standing controversy over the amount of reddening of AGNs. McKee & Petrosian (1974) argued against significant amounts of reddening in quasars on two grounds. The first was the apparent lack of the strong λ2175 extinction hump (e.g., Pitman, Clayton, & Gordon 2000), and the second was the lack of curvature of the UV continuum. Cheng, Gaskell, & Koratkar (1991) found that the ultraviolet slopes for a wide variety of AGNs at high and low redshift, high and low luminosity, and differing radio types were essentially the same to within their measuring errors. They limited line-of-sight reddening to E($B-V$) $\sim$ 0.1 mag (assuming a Galactic reddening curve). In the optical, on the other hand, there is clear evidence at least for significant reddening in the host galaxy plane. De Zotti & Gaskell (1985) showed that both the lines and continua of radio-quiet AGNs (Seyfert galaxies) with axial ratio a/b are typically reddened by E($B-V$) $\sim 0.2(a/b)$ mag. Also, unified models of both radio-loud and radio-quiet AGNs require significant dust extinction in a nuclear torus (tipped with respect to the spiral host; see Antonucci 1993) and this must produce detectable effects on spectra of both radio-loud and radio-quiet AGNs.

Reddening curves have been determined for the radio-quiet AGNs NGC 3227 (Crenshaw et al. 2001), and Ark 564 (Crenshaw et al. 2002) by assuming that they have the same underlying continuum as other, bluer AGNs. These reddening curves show little or no λ2175

bump and rise *more* steeply in the far UV than the standard Galactic reddening curve (i.e., they resemble the reddening curve of the SMC). Crenshaw et al. (2001, 2002) argue that the dust in NGC 3227 and Ark 564 is outside the narrow-line regions and hence far removed from the nuclei. Similarly, Richards et al. (2003) show that SMC-like reddening affects the spectra of a few percent of radio-quiet quasars. In this paper we determine mean reddening curves for large samples of radio-loud and radio-quiet quasars, and argue that *most* quasars are also affected by substantial extinction which has a quite flat reddening curve in the UV. This curve is qualitatively different from any previously proposed reddening law. We explore the significance of this result for our understanding of AGNs.

2. THE REDDENING CURVE

2.1. The Sample

Baker & Hunstead (1995) present composite Anglo-Australian Telescope optical and (rest-frame) UV spectra of 72 FR II radio quasars and broad line radio galaxies from the Molonglo Quasar Sample (MQS). The data have the advantages of being homogenous and being selected almost exclusively by radio-lobe flux, a nearly isotropic parameter. They also have broad optical/UV wavelength coverage, typically over a rest-frame wavelength range of $\sim$ 2000 Å to $\sim$ 5000 Å, depending on redshift. Radio core-to-lobe flux ratios, $\Re$, were measured from 5 GHz VLA maps. Baker & Hunstead excluded a few AGNs from the sample because of abnormally strong absorption features, a lack of $\Re$-values, or a BL Lac type featureless spectrum. They grouped the AGNs into four subsets chosen according to $\Re$-values and radio structure, creating composite UV-optical spectra of 13-18 objects each. The four subsets are $\Re \geqslant 1$, $0.1 \leqslant \Re < 1$, $\Re < 0.1$ and Compact Steep Spectrum (CSS) radio sources. Baker & Hunstead (1996) also give mean line strengths for the four subsets. In addition to the MQS AGNs we also considered the similar quality predominantly radio-quiet Large Bright Quasar Survey (LBQS) composite spectrum of Francis et al (1992), based on the spectra of 1018 quasars.

2.2. Method and Justification of Method

Our continuum extinction curves are derived by division of pairs of composite continuum spectra, on the assumption that the intrinsic continua are the same. While this is routinely done for stars of a given spectral type, there is in principle a huge risk in applying this method to AGN. Stars with matched classifications almost certainly have intrinsically similar spectra,

but there is no guarantee that one AGN composite is intrinsically similar to another. In fact for the AGN case, variability appears to affect the spectral shape so the intrinsic matches cannot be perfect for that reason alone. However, the averaging within the composites will greatly reduce the last problem. Note that our sub-samples are matched in radio-lobe power.

We also determined the reddening curve for the broad-line region (BLR) lines in the samples. In doing this we are, again, assuming that there are no intrinsic object-to-object BLR differences. This is certainly not true for individual objects but again we hope that the large number of AGNs in each subset minimizes the uncertainties introduced.

There are two very good pieces of evidence we will present that reddening (rather than intrinsic spectral differences) does in fact drive most of the observed spectral differences. The first is that a *single* reddening curve shape reconciles the shapes all four radio composites.

More importantly, we shall see that *the reddening curves derived from the continua and separately from the broad emission lines have nearly the same shape and amplitude.* Changing physical conditions in the BLR cannot mimic reddening when many lines are considered together [1].

As explained at the end of this paper, the validity of our conclusion will soon be tested in a simple robust manner: it predicts powerful infrared emission for the lobe-dominant radio-loud quasars, far exceeding that of the blue-selected PG radio-quiet quasars.

2.3. Results

2.3.1. Choice of Comparison Groups

There are four radio quasar samples considered in the paper: core-dominant classical doubles, intermediate classical doubles, lobe-dominant classical doubles, and compact-steep-spectrum sources. Roughly speaking, the current wisdom is that the first three classes differ from one another only in orientation, while the last class comprises sources which are intrinsically different, in particular being much smaller physically.

We concentrate on two comparisons among the groups. First, we compare the core-dominant versus the lobe-dominant sample. There is empirical and theoretical evidence that the latter are more reddened, so such a comparison should reveal the shape of that reddening.

The compact-steep-spectrum quasars are thought to range widely in orientation. They

[1]However, a single line pair alone often gives ambiguous results – see Grandi (1982).

fill the parameter (viewing angle) space of all three groups of classical double radio quasars considered above[2] Thus, if we are to compare them to a subgroup of the classical doubles, it would be best to select the subgroup at intermediate orientation as we have done. One might compare them to a composite of all the classical doubles, but restricting the comparison group to those at intermediate orientation has another very important advantage: our two comparisons and thus our two reddening curves for the radio loud population are strictly independent of each other, with no objects in common. Thus their mutual agreement cannot be an artifact of interdependent samples.

2.3.2. Reddening Curve Comparisons

We derived relative reddening curves for two independent pairs of sub-samples of the four composite spectra given by Baker & Hunstead. We compare the $\Re \geqslant 1$ ("face-on") sample with the $\Re < 0.1$ ("edge-on") sample, and the $0.1 \leqslant \Re < 1$ ("intermediate-orientation") sample with the CSS sample. We avoided prominent spectral features (like major broad or narrow emission lines and absorption troughs) or, in some cases, we made interpolations over residual absorption features and noisy regions of the spectra. We also determined the extinction curves for the BLR using the mean line strengths given in Table 1 of Baker & Hunstead (1996a,b). Because of the difficulty of measuring BLR strengths due to the wings of the lines the uncertainties are larger for the BLR lines than for the continua. In Figure 1 we show each of the $E(\lambda - V)$ curves normalized to $E(B-V) = 1$. Of course the uncertainty in the normalization in the optical introduces some uncertainty in the level of the UV curves.

The two continuum extinction curves, coming from the two totally independent data subsets, agree well, especially since we have only matched the curves in the optical region, rather than using a globally-optimal scaling to get the best overall match. It is important to note that the BLR extinction curve is also consistent with the two continuum curves[3].

All three reddening curves are extremely flat in the UV. This is very different behavior from the standard Galactic reddening curve (with a ratio of total to selective extinction, $R_V = 3.1$) shown for comparison in Figure 1. It is also very different from the Small

[2]Note that the *edge-on* quasars are thought to be optically-obscured and to manifest themselves as radio-galaxies.

[3]It should be noted that our scenario therefore allows us to explain much of the high observed ratios of Balmer line strengths to Ly α by extinction. These ratios are still dependent on physical conditions in the BLR however, as is shown by variations of the Balmer to Ly α line ratios across line profiles (see Snedden & Gaskell 2004).

Magellanic Cloud (SMC) reddening curve that has also been considered as a possible form of the wavelength dependence of the extinction in AGNs (Crenshaw et al. 2001, 2002). Reddening by a galactic curve or an SMC curve turns a power-law into a convex spectrum (see McKee & Petrosian 1974) while our nuclear reddening curve produces a concave spectrum. As noted in the Introduction, Richards et al. (2003) find that a few percent of the SDSS (mostly radio-quiet) AGN are significantly affected by SMC-like reddening and our results are consistent with that. Richards et al. state that attempting to explain their large color-segregated composites generally with reddening "results in good matches at both 1700Å and 4040Å, but over predict(s) the flux between these two wavelengths and under predict(s) the flux shortward of C IV." This is exactly what is predicted by our reddening curve in Fig. 1, and qualitatively confirms that our picture appears to be very broadly applicable.

A flat extinction curve implies large grain sizes relative to the wavelengths involved. We note in fact that Galactic reddening curves from regions having a large value of the total extinction to selective extinction ratio, $R_V \sim 5$, such as the line of sight to the star formation region Herschel 36 (Fitzpatrick & Massa 1988), do give flat UV extinction curves. The major difference between the Herschel 36 reddening curve and our radio-loud quasar curves is the absence of the λ2175 absorption feature in our curves. For comparison, we show a parameterized extinction curve with $R_V = 5.30$ (a good fit to the Herschel 36 line of sight), and a "normal" extinction curve. Both curves are taken from Cardelli, Clayton & Mathis (1989, hereinafter CCM89).

Next, we consider the predominantly radio-quiet (and blue-selected) LBQS survey objects. Figure 2 shows the relative reddening curve between the composite spectrum from Francis et al. (1992) and the relatively unreddened $\Re \geqslant 1$ composite of Baker & Hunstead (1995). This shows the excess reddening relative to this radio-loud sample. Since the LBQS composite spectrum is rather noisy in the V-band, we did the normalization to $E(V-V) = 0$ and $E(B-V) = 1$ by doing a fit to the four data points with lowest frequencies. The resulting reddening curve is significantly steeper than the radio-loud reddening curves in Figure 1, but not quite as steep as the Galactic reddening curve, or the NGC 3227 and Ark 564 reddening curves of Crenshaw et al (2001, 2002). Again, there is the lack of the λ2175 bump. In fact, there is an apparent dip in the reddening curve around the λ2175 bump. This would be hard to understand physically unless there were a scattering component to the λ2175 extinction feature. We suspect instead that this is due to a break down of our assumption that the intrinsic continua are the same for the samples. This could be a consequence of a difference in the UV Fe II emission. Part of the well-known Boroson & Green (1992) "eigenvector-1" correlations (which include differences between radio-loud and radio-quiet AGNs) is variation in the Fe II emission, and the Fe II emission is important in the so-called "small blue bump" (SBB) continuum around $\lambda^{-1} \sim 3.5$. De Zotti & Gaskell (1985) discuss the effects

of Fe II on measurement of a λ2175 absorption feature. Note that in deriving the reddening curves there is no reason to exclude SBB emission, which arises in the BLR; the dust affects it the same way as the BLR and continuum source. While λ2175 has almost always been reported to be weak in AGNs, it should be noted that De Zotti & Gaskell (1985) did find a correlation between their estimated reddening and published strengths of the λ2175 feature (see their Table 3 and their Fig. 12) for dust in the host galaxy plane of Seyferts. There are also occasional reports (e.g., Grossan et al. 1996) of a significant λ2175 feature in quasars.

2.4. The Ratio of Total to Selective Extinction (R_V)

We estimated R_V for our extinction curves by two methods. First we followed the standard approach of extrapolating E_λ to $\lambda^{-1} = 0$. Actual measurements of E_λ in the IR are not available and would give inaccurate results anyhow because of the onset of IR emission from dust. Therefore, following the procedure of CCM89, we extrapolated to $\lambda^{-1} = 0$ by assuming that the IR reddening curve has the same shape as the Galactic curve of Rieke & Lebofsky (1985).[4] To match Rieke & Lebofsky (1985) we converted our curves to A_λ/A_V using the relation:

$$A_\lambda/A_V = \frac{A_\lambda - A_V}{A_V} + 1 = \frac{A_\lambda - A_V}{R_V \cdot E(B-V)} + 1 = \frac{1}{R_V} \cdot \frac{E(\lambda - V)}{E(B-V)} + 1.$$

We show one of our radio-loud A_λ/A_V AGN extinction curves together with the infrared data of Rieke & Lebofsky (1985) in Fig. 3. We allowed the Galactic curve to vary by a scale factor C (see CCM89). By assuming a similar shape for the AGN and Galactic sample, we obtain R_V.

CCM89 show that the main variations in Galactic optical-to-UV extinction laws are a function of R_V alone and this gives another way to find an estimate of R_V. In order to use the CCM89 relationships for our extinction curves, we had to modify their relationships for the optical/near-UV branch to account for the lack of the λ2175 feature. For $3.3\mu m^{-1} \leq x \leq 8\mu m^{-1}$ with $x = \lambda^{-1}$ we hence defined the function $\bar{b}(x)$ as

$$\bar{b}(x) = -3.09 + 1.825x + 1.5/[(x - 4.62) + 0.85] + F_b(x)$$

instead of function 4b in CCM89. We adjusted R_V in the modified CCM89 approximations until they fit our extinction curves. From this we get two estimates of R_V, one from the fit to the optical/near-UV range and the other from the fit the far-UV branch. We

[4]The IR reddening is relatively low, and known reddening curves differ only slightly in that region, so this is probably safe

summarize our resulting R_V values in Table 1.

Within our estimated errors, all three wavelength ranges (IR, UV/optical, and far-UV) lead to similar estimates of R_V, and all R_V values for our radio-loud curves are significantly greater than the canonical Galactic value of 3.1.

For NGC 3227 Crenshaw et al. (2001) obtained $R_V = 3.2$ and for Akn 564 Crenshaw et al. (2002) obtained $R_V = 3.1$. Both of these are very close to the Galactic value, but these Seyfert curves likely refer to a non-nuclear environment.

Some additional support for the flat shape of our reddening curves in the UV comes from the lack of luminosity dependence of UV slopes found by Cheng et al. (1991), and the sharp upper limit to the $\lambda 4220/\lambda 1460$ ratio found by Malkan (1984). We discuss this in section 4.

3. THE CONTINUUM SHAPE AND DEGREE OF REDDENING IN AGNS

In deriving the extinction curves for the radio quasars in the previous section, we started by assuming that the optical/UV-continuum shapes were the same *for each pair* of composites. This, by construction, leads to inferred intrinsic spectra which match each other for each pair. But what is *not* true by construction, and what argues for a rather generic reddening law, is that the two continuum extinction curves, derived from independent data, agree with each other in shape, as can be seen in Figure 1. More remarkably, as can also be seen in Figure 1, the continuum reddening curves for each pair agree in both shape and amplitude with curves derived from the *emission lines*. Again, this is not true by construction, but argues for a correct and generic extinction law. To summarize: both independent continuum pairs lead to the same extinction curve, and the corresponding emission lines produce an extinction curve which also agrees in shape and amplitude.

There is already evidence for a universal spectral energy distribution in radio-quiet AGN. In Fig. 4 we show the $\lambda 1600/\lambda 4220$ spectral index, α_{UVO} (for $F_\nu \propto \nu^{-\alpha}$), for radio-quiet AGNs in three optical luminosity bins in L_{4200} (in erg sec^{-1} Hz^{-1}). We have calculated these from data in Malkan (1984) and references therein. We only show spectral indexes for objects with simultaneous or nearly simultaneous UV and optical observations. The observations were already corrected for Galactic reddening using $E(B-V)$ values from Burstein & Heiles (1982) and assuming a standard Galactic reddening curve.

For the highest luminosity sample ($|\log L| > 30.5$), the mean α_{UVO} is 0.54, and the standard deviation is only 0.064. If this small dispersion is due to reddening, it corresponds

to E(B-V) ~ 0.06, assuming a reddening curve like our Fig. 1, or to E(B-V) < 0.02, if we assume a standard Galactic reddening curve. Thus, as was argued by Malkan (1984), the intrinsic extinction in these high-luminosity AGNs is probably very low.

For the radio-quiet AGNs with $29 < |\log L| < 30.5$, the important thing to note is that the *cutoff at* $\alpha_{UVO} \sim 0.45$ *is the same as for the highest luminosity AGNs*[5]. Both reddening and contamination by starlight from the host galaxy will increase α_{UVO}. For $|\log L| < 29$ we see again that *there is the same cutoff at* $\alpha_{UVO} \sim 0.45$. As noted by Malkan (1984), the constancy of the cutoff slope in the face of a difference in the mean slope can be totally explained by increasing the host galaxy contamination and reddening. However, when we compare reddenings from the optical and UV (see below), we will see that reddening, not host galaxy contamination is the dominant factor. The cutoff at $\alpha_{UVO} \sim 0.45$ is presumably the unreddened value. *It is remarkable that this is the same over more than 4 orders of magnitude in luminosity.* It would be hard to explain the increasing spread in spectral index with decreasing luminosity as an intrinsic luminosity effect given that the *cutoff* is independent of luminosity.

Ward et al. (1987) argue that all AGN continua are the same and that differences are due to reddening and host galaxy starlight contamination. For low-redshift, radio-loud quasars, Netzer et al. (1995) showed that there is a correlation between the observed $Ly\alpha/H\beta$ line ratios and the $\lambda 1216/\lambda 4861$ continuum flux ratios. This is evidence for radio-loud quasars having similar unreddened continuum shapes and similar hydrogen-line ratios. The bluest $\lambda 1216/\lambda 4861$ flux ratio on the reddening vector in their Fig. 6 is 8.7. This implies $\alpha_{UVO} \sim 0.44$ and supports the idea of a universal $\alpha_{UVO} \sim 0.45$. However, Bechtold et al. (1996) found a similar correlation (for the same wavelength range) for high-redshift predominantly radio-quiet AGNs but the blue end of their reddening vector gives $\alpha_{UVO} \sim 0.2$.

Assuming that the bluest AGNs have $\alpha_{UVO} = 0.45$, and adopting our radio-loud-AGN reddening curve, the mean reddenings (E(B-V)) of the four Molongo samples, going from "face-on" to CSS are, 0.29, 0.34, 0.71, and 0.98 mag. (with formal relative uncertainties of about ± 0.06). If the "face-on" sample is assumed to be unreddened then the mean reddenings are 0.00, 0.05, 0.41, and 0.69 magnitudes respectively, but this requires the unreddened $\alpha_{UVO} = 0.70$. We consider this highly unlikely since we get flatter (bluer) *observed* spectral indices from the Netzer et al. (1995) measurements. Since the reddening curve for the predominantly radio-quiet LBQS sample appears to be different, we derived the reddening

[5]Of course, our slopes cannot be compared directly with published values defined differently. For example, Richards et al. (2003) quote "photometric" spectral indices, measured using fixed observed-frame optical bands, with only statistical corrections for emission and absorption features. Many widely varying spectral index prescriptions are used in the literature.

from the long wavelength region (i.e., the optical) of the spectrum only. This gives a mean E(B-V) $\sim$ 0.30 mag (i.e., similar to the face-on Molongo radio-loud AGNs) if we assume that the unreddened $\alpha_{UVO} = 0.45$. Ward & Morris (1984) got E(B-V) $\sim$ 0.3 for NGC 3783; Crenshaw et al. (2001) got a total E(B-V) of 0.20 for NGC 3227; and Crenshaw et al. (2002) got a total E(B-V) of 0.17 for Ark 564. All three of these are in the range considered here.

Needless to say, the lower apparent reddenings of radio-quiet, and hence, usually optically-selected, AGNs must be strongly influenced by selection effects. It would be interesting to study the reddenings of X-ray selected samples of radio-quiet AGNs.

It should be noted that after de-reddening with our reddening curve, there is no difference between the spectral energy distribution of CSS sources and other AGNs. The apparent weakness of the SBB in CSS sources is simply a consequence of the high degree of reddening and the shape of the reddening curve which has its greatest curvature at the position of the SBB. Our reddening curve might similarly explain the unusual spectral shapes of some broad-absorption line quasars without the need to invoke partial covering (see Hall et al. 2002).

4. LUMINOSITY DEPENDENCE OF REDDENING

Assuming, as we have argued in the previous section, that the intrinsic continuum really is independent of luminosity, we can use our nuclear reddening curve to investigate the luminosity dependence of the reddening. In Fig. 5 we show the luminosity dependence of the reddenings, calculated from the UV to optical slope (as discussed in the previous section) and from the optical λ4200 to λ7000 slopes given by Mushotzky & Wandel (1989). It should be noted that the Malkan (1984) and Mushotzky & Wandel (1989) samples are two different heterogenous samples. We have assumed that the spectra are unreddened for the highest luminosities. The error bars are the errors in the means ($\sigma/\sqrt{(}n)$.)

The first thing to notice from Fig. 5 is that the reddenings, derived by the two methods, and from the two different samples, are in rough agreement. The differences in the reddenings deduced by the two methods for the two lowest luminosity bins are comparable to the scatter in the reddening curve in Fig. 1. Although the differences exceed the formal $\sigma/\sqrt{(}n)$ error bars, we consider the two derivations to be in satisfactory agreement. There would not be this level of agreement had we used a reddening curve which is more selective in the UV. For example, had we used the standard Galactic reddening curve, the reddenings derived from the UV-optical slope (the solid squares) would then be more than a factor of two lower. This suggests that our proposed nuclear reddening curve is more realistic.

It is important to recognize that the agreement in reddenings deduced from the two spectral regions would also not occur if the steepening of spectral indices at lower luminosities were due to increasing host galaxy contamination. To illustrate this, in Table 2 we show the reddenings, E(B-V), that would be inferred using our reddening curve if host galaxy contamination were interpreted as reddening. We approximated an unreddened AGN continuum as an $\alpha = 0.45$ power-law and added in host galaxy contamination assuming the composite spiral galaxy SED in Table 6 of Schmitt et al. (1997). Using their elliptical SED makes no significant. We then interpreted the changes in flux ratios as a reddening. The first column in Table 2 shows the ratio of AGN to galaxy flux at 7000 Å. The last two columns give the corresponding reddenings inferred using our reddening curve.

As can be seen from Table 2, if host galaxy contamination were to be mistaken for reddening, the reddenings inferred from the UV-optical would always be greater than those inferred from the optical alone. Host galaxy contamination would produce an offset between the optical-reddening and optical-only reddening in the *opposite* sense to the slight difference shown in Fig. 5. Two factors are responsible for host galaxy contamination leading to greater apparent reddenings from the optical than from the optical-UV. First, the SED of a host galaxy is steeper from the optical to the UV than it is in the optical alone. Second, similar changes in UV-optical color and optical color correspond to a larger change in the E(B-V) deduced from the UV-optical color because our reddening curve is flatter from the optical to the UV than it is in the optical region alone.

The differences in Fig. 5 between the reddenings deduced from these two spectral regions could be due to departures from our reddening curve (e.g., because of reddening by additional extra-nuclear dust), but they could equally well be due to differences in the samples. The Malkan (1984) sample is predominantly optically selected, and hence biased towards lower reddening objects; the larger Mushotzky & Wandel (1989) includes a large fraction of radio-loud (and thus radio-selected) AGNs.

The second thing to notice from Fig. 5 is that the reddenings derived by both methods increase monotonically with decreasing luminosity. Mushotzky & Wandel (1989) attributed the steepening of the optical slope to intrinsic differences in the spectral shapes, perhaps due to differing black hole masses and accretion rates (Wandel & Petrosian 1988). However, using our reddening curve, we can accurately predict the luminosity dependence of the optical slope in Mushotzky & Wandel (1989) entirely from the UV-optical reddening. We are not ruling out the possibility that there are luminosity dependencies in the intrinsic (de-reddened) continuum shape. Before these can be found, we must account for the dominating effect of reddening. Another prediction is that if the dust has a reddening curve similar to that in Fig. 1, then the lowest luminosity objects should show *concave* SEDs going from the near

IR to the far UV.

Variations in the degree of reddening from object to object naturally explain the spread in continuum shapes at a given luminosity. In Fig. 4 it can be seen that as the mean spectral index increases, so does its spread. If the continua are unreddened and the differences in continuum shape are intrinsic, perhaps due to differences in black hole mass and accretion rate, then the wide range of spectral indices at lower luminosity is hard to understand.

5. THE RELATIONSHIP BETWEEN THE X-RAY AND OPTICAL EMISSION

5.1. Luminosity dependence of L_X/L_{opt}

It is long been known that the observed ratio of X-ray to optical luminosity is a decreasing function of optical (or UV) luminosity (Reichert et al. 1982, Zamorani et al. 1982, Avni & Tananbaum 1982, Kriss & Canizares 1985) with $L_X \propto L_{opt}^{0.70-0.85}$. This has generally been attributed to luminosity-dependent physical conditions in the AGNs themselves. In contrast to the relationship between L_X and L_{opt}, Malkan (1984) showed that $L_X \propto L_{IR}$. Mushotzky & Wandel (1989) reconciled these results by showing that the dependence of L_X on the luminosity at longer wavelengths depends on where the longer wavelength luminosity is measured. We believe instead that the L_X/L_{opt} ratio appears to vary simply because the greater extinction in lower luminosity objects causes the optical luminosity to appear to be lower than it really is, while X-ray luminosities at $\gtrsim$ 2keV are unaffected. We quantitatively tested this by using $L_X \propto L_{opt}^a$, to predict the observed optical luminosity, then assuming that the intrinsic optical luminosity was proportional to L_X, and using this to predict the reddening using our reddening curve. The luminosity dependence of the reddening seen in Fig. 5 is well matched with $a \sim 0.8$. Going in the other direction, and assuming the luminosity dependence in Fig. 5, we predict that there should be some curvature in the L_X vs. L_{opt} plot. This should be detectable with well-defined samples.

5.2. Dependence of L_X/L_{opt} on Radio-loudness

Zamorani et al (1982) reported that radio-loud AGNs are about three times as luminous in X-rays as radio-quiet AGNs of the same observed optical luminosity. According to the arguments of the present paper, much of this difference must result from a denominator in L_X/L_{opt} reduced by dust absorption. A factor of three corresponds to a difference in E(B-V) of ~ 0.25 – 0.35 (depending on R_V). This is similar to the radio-loud/radio-quiet differences

we find in optical absorption using our reddening curve (see above).

This is not the whole story however, because Zamorani et al (1982), Kembhavi (1994), Shastri (1997), and Brinkmann et al 1997, among others, have argued that there is at least some beamed contribution to the L_X/L_{opt} difference, because the numerator is enhanced by a beamed component in the radio-loud objects with strong cores. The clinching argument here is that core-dominant objects often have harder X-ray spectra (Brinkmann et al. 1997), heralding the arrival of a new spectral component, but this observational effect is modest in size and ubiquity. We note that Sambruna, Eracleous, & Mushotsky (1999) find that X-ray slopes are similar for radio-loud and radio-quiet AGNs when the samples are matched in luminosity.

A quantitative assessment of the relative importance of X-ray beaming and optical absorption to the enhanced L_X/L_{opt} in radio-loud AGNs is far beyond the scope of this paper. We simply state here that, if we are correct, a significant part of the higher average L_X/L_{opt} in radio-loud AGNs must be due to a denominator diminished by optical absorption in many cases, and this must be accounted for as well as the beaming.

6. DISCUSSION

6.1. Evidence for Larger Grain Sizes

The simplest explanation of the flat UV extinction curves we find is that small grain sizes are depleted relative to the grain-size distribution in our galaxy. There is other evidence for depletion of small grains. It has long been known that the optical extinction in AGNs is considerably less than is predicted by the X-ray column densities (Maccacaro, Perola & Elvis 1982, Reichert et al. 1985). By comparing the reddening of optical and infrared broad lines and the X-ray absorbing column density Maiolino et al. (2001b) find that the $E(B-V)/N_H$ ratio is nearly always lower than the Galactic values by a factor ranging from ~ 3 up to ~ 100. They argue that this cannot be due to conversion of refractory elements to the gas phase but is instead caused by larger grains. Sambruna et al. (2002) find that approximately 50% of BLRGs have columns of cold gas comparable to the columns detected in NLRGs. This suggests that the small grains are depleted in gas swept off the torus.

The silicate feature at $9.7\mu m$ observed in the mid-IR spectra of many Galactic sources is absent in the average ISO spectrum of a sample of Seyfert 2 galaxies obtained by Clavel et al. (2000). Maiolino, Marconi, & Oliva (2001a) conclude that the most likely explanation of this is that dust in the circumnuclear region of AGNs is predominantly composed of large grains that do not contribute to the feature at 9.7 μm. Imanishi (2001) has argued from the

probable shape of the IR L and M' band extinction curve that it is due to large grains.

There are other good arguments that small grains are severely depleted in gas swept off the torus. On the observational side, we are confident that free electrons sometimes dominate the scattering above the torus (Miller, Goodrich, & Mathews 1991; Ogle et al 2003). Small grains have orders of magnitude greater scattering efficiency per gram of ionized Galactic interstellar medium compared with electrons, so they must be very thoroughly eliminated for electrons to dominate. In section 6.3 we discuss ways in which small grains can be destroyed close to an AGN.

6.2. Modelling Extinction Curves for AGN

Mathis, Rumpl & Nordsieck (1977, MRN) suggested compositions and grain size distributions for Galactic interstellar dust. A possible realization of their model contains two sorts of dust with differing optical properties: carbonaceous or "graphite" grains, making up 37.5% and "astronomical silicate" making up 62.5%. This dust composition reproduces the interstellar media extinction curve fairly well.

Weingartner & Draine (2001) developed the MRN model to construct size distributions for carbonaceous and siliceous grain populations in different regions of the Milky Way and Magellanic Clouds. They present distributions that reproduce the observed extinction through various lines of sight. The $\lambda 2175$ feature is caused predominantly by *small* carbonaceous grains. Inspection of their results shows that extinction curves such as we find can be naturally explained by a relative lack of both small carbonaceous and small siliceous grains.

We modelled our AGN extinction curves using a computer code which calculates extinction cross sections from Mie theory. Such a code is given by Bohren & Hufman (1983). It is based on the solution of the Maxwell equations for radiation scattering by a spherical grain with defined radius a and dielectric constant ϵ. A graphite grain has differing optical properties for radiation propagating parallel or perpendicular to the symmetry axis of the crystal. The model takes care of this difference by using two different kinds of graphite grains, $G_{r_\parallel}$ and $G_{r_\perp}$. Considering three spatial dimensions there has to be twice as much $G_{r_\perp}$ as $G_{r_\parallel}$. Further details of our procedures can be found in Goosmann (2002). In the standard MRN model the number density $n(a)$ of grains with radius a follows a $n(a) \sim a^{\alpha_s}$ law, with $\alpha_s = -3.5$, minimum grain size $a_{min} = 0.005 \mu m$ and maximum grain size $a_{max} = 0.250 \mu m$. Based on this grain size distribution MRN were able to compute the standard extinction curve for our Galaxy.

We recalculated the standard extinction curve and then varied the dust composition,

grain size limits and α_s. We found that the slope of the UV extinction curve tends to be determined by a_{min} whereas the level of $E(\lambda - V)$ in the UV varies more with α_s. In Fig. 6 we show a fit to our reddening curve. In order to achieve good agreement we lowered the abundance of graphite to 15% of the graphite/silicate mixture. In addition to this we raised α_s to -2.05 and lowered a_{max} to $0.200\mu m$.

A possible physical basis for this grain-size distribution is the following: when a standard Galactic dust cloud is irradiated by hard quasar radiation small grains are preferentially destroyed, and larger grains are partly depleted. Therefore the upper limit of the grain radii should go down. The lower limit stays the same because the destroyed small grains are replaced by depleted larger ones. Hence there is always a fraction of small grains. However, since larger grains have a better resistance against the destruction processes, their relative abundance rises and so does α.

It is hard to explain why the fraction of carbonaceous dust is lower than in the MRN model since graphite actually has a higher sublimation temperature than silicate. The hard quasar radiation should preferably destroy silicate. This might be a limitation of our model where the only way to lower the $\lambda 2175$ feature is by decreasing the carbon abundance. In reality there might be another carbonaceous substance, such as PAH molecules, not included in our modeling, which is predominantly producing the $\lambda 2175$ feature.

We have made no attempt to model the reddening curve we found for radio-quiet AGNs because we suspect that the differences between this and the radio-loud reddening curve are caused by additional reddening further out in the host galaxy while the "nuclear" dust is similar. The dust further out would have more "Galactic" properties than the nuclear dust.

It should be noted that our "nuclear" reddening curve is for external line of sight reddening of a single point source. This is quite different from the case of starburst galaxies (Calzetti, Kinney, & Storchi-Bergmann 1994) where the dust is mixed in with multiple sources, each with different extinctions, and where geometrical effects in the complex environment affect the shape of the reddening curve. Those effects can eliminate the strong spectral curvature and exponential cutoff otherwise mandated by the usual reddening curves. In our case there are no exponential cutoffs despite the extinction being in the *foreground*.

6.3. Mechanisms for Depleting Small Grains

There are many mechanisms that can selectively destroy small grains. Gas in the outer regions of dense clouds in our galaxy is observed to have a higher relative abundance of larger grains (Mathis 1990), and this is believed to be due to coagulation of smaller grains.

Gas near an AGN is close to the sublimation radius, and small grains can be destroyed by single-photon heating. Absorption of a single X-ray photon will eliminate grains of radius $< 10\mathring{A}$ and deplete grains several times larger than this (Laor & Draine 1993). As we have already mentioned in section 6.2, Siebenmorgen et al. (2004) have shown how soft X-rays destroy PAH molecules. Small grains have a shorter lifetime due to thermal sputtering (Draine & Salpeter 1979). Smaller grains can also be efficiently destroyed by acquiring a high positive charge from the photoemission of electrons in the intense hard radiation field of AGNs (Draine & Salpeter 1979; Chang, Schiano, & Wolfe 1987). The high positive charge of large grains will also suppress thermal sputtering. If the AGN is not radiating far below the Eddington limit, grains will be efficiently accelerated away from the black hole. The ratio of radiative acceleration to gravitational acceleration is $\propto a^{-1}$, where a is the grain radius, so smaller grains will be expelled faster (see Draine & Salpeter 1979). The faster moving grains will also be subject to enhanced sputtering (Laor & Draine 1993).

6.4. Continuum Variability

In section 3 we have presented evidence for similarity of the average continuum shapes of a wide variety of AGNs. We are not, however, arguing for a precisely standard spectral energy distribution. It is widely reported that as AGNs vary, α_{UVO} changes, being steeper in low states (e.g., Perola et al. 1982). However, much of the observed effect derives from a constant component from the host galaxy. Also contributing is the SBB atomic feature, which responds to continuum changes with reduced amplitude and a time delay. Korista & Goad (2001) recently showed that atomic continua can cover a much wider spectral region than just the SBB.

On the other hand, small delays have been reported between the UV flux and the optical (Collier et al. 1998, 2001; Kriss et al. 2000; Collier 2001, Oknyanskij et al. 2002; Gaskell et al., 2004). While there have been cases of reported steepening of the UV spectrum as AGNs have varied, it is notable that in the case of Fairall 9 *the UV continuum slope stayed the same* at 0.46 ± 0.11 while the UV flux changed by a factor of over 20 (Clavel, Wamsteker, & Glass 1989).

Where the continuum does steepen as it fades, it is possible that the extinction has changed (Barr 1982). If this is the case it would be due to compact dust clouds moving across the line of sight. There is support for this idea from the frequently-seen variations in X-ray column densities on timescales of less than a year (e.g., Risaliti, Elvis, Nicastro 2002), and the temporal variations in the position angles of the polarizations of broad lines in AGNs (e.g., Goodrich 1989, Martel 1998) which imply motions of the scattering dust clouds near

the broad line region. More directly, Goodrich (1989) showed that the Balmer decrements and continuum slopes change simultaneously in a way consistent with varying reddening.

However, changing extinction is far from the whole story of variability, since the X-rays vary, and often correlate with the optical/UV (see Gaskell & Klimek 2003 for review).

6.5. Absorption Lines

Dust is associated with gas, so if optically steep AGN spectra are caused by reddening then we would expect that "red" AGNs would show stronger absorption. Wills et al. (2000) have indeed found that AGNs with strong UV absorption lines have redder optical-UV continua and either weaker or flatter soft X-ray continua. Baker et al. (2002) in their study of associated C IV absorption also found that heavily-absorbed quasars are systematically redder and they found that C IV associated absorption is found preferentially in steep-spectrum and lobe-dominated quasars. The Wills et al. (2000) and Baker et al. (2002) results provide additional independent support the idea that changes in continuum shape are due to dust.

7. CONCLUSIONS

If our reasoning is correct, we can draw several important conclusions about AGNs.

1. The reddening curve for radio-loud AGNs has a fairly universal and unprecedented shape, being quite flat in the UV but selective in the optical.

2. The observed reddening of radio-quiet quasars is somewhat more selective in the UV relative to the optical, compared with radio-loud AGNs but this could well be because of additional dust far out in the host galaxy.

3. Even though most well-studied quasars show no UV curvature, much of their radiated energy is in fact absorbed.

4. The flat nuclear reddening curve in the UV can be straightforwardly explained by grain destruction depleting the number of small grains, a notion consistent with many arguments in the literature.

5. The normalization (average amount of extinction) for lobe-dominant quasars on average decreases with radio core dominance, as anticipated by Baker et al (1997) and Baker and Hunstead (1995). There is powerful evidence from radio astronomy that this means that

absorption increases with line-of-sight inclination to the radio jets, as expected qualitatively in the standard "unified model" (Wills 1999).

6. Compact Steep-Spectrum (CSS) radio quasars have the same type of extinction curve and high reddening.

7. The continuum shapes of all but the bluest quasars are affected by reddening, and are intrinsically similar to those of the bluest quasars.

8. The average reddening decreases substantially with increasing luminosity.

9. The luminosity dependence of extinction explains most or all of the luminosity dependence of L_X/L_{opt}, and the variation of this dependence with the choice of optical wavelength.

10. Differences in reddening are also a major factor in the difference in L_X/L_{opt} between radio-loud and radio-quiet AGNs.

11. If they are correct, many of these results are of vital importance for demographic studies (intrinsic luminosity density of AGNs in the universe), and for modelling the crucial Big Blue Bump continuum component of AGN.

The most satisfying thing about the results from this paper are they are readily and robustly testable. The nearly unequivocal prediction is that radio-loud quasars must be generally powerful thermal radiators. This is especially true for those with steep optical slope, despite their general lack of exponential UV cutoffs as expected in the case where small grains are present. While the exact infrared luminosities are model-dependent, only predictable statistically, and far beyond the scope of this paper, they should generally be energetically very important, and often dominant. The one obvious caveat is that the optical/UV radiation may be intrinsically emitted anisotropically, as has been argued on other grounds by Miller, Goodrich, & Mathews (1991) among others. This could reduce the amount of re-processed radiation.

We are grateful to Mark Bottorff, Patrick Hall, Ari Laor, John Mathis, Dick McCray, Rita Sambruna, Joe Shields, Joe Weingartner, & Adolf Witt for useful comments and discussion. This research was supported in part by NSF grant AST-0098719 and by the Hans-Böckler-Stiftung.

A. AN AGN EXTINCTION CURVE

In Table 3 we give an average extinction curve for the optical and the UV waveband. It is based on Fig. 1 and we have tabulated it at the wavelengths of major emission lines as well as the B and the V band. Note that values for wavelengths corresponding to x outside the range 1.6–8 μm^{-1} are extrapolated.

The reddening curve can be represented analytically by the following functions of $x = \lambda^{-1}$ in μm^{-1}:

$$A_\lambda/A_V(x) = -0.8175 + 1.5848x - 0.3774x^2 + 0.0296x^3, \quad 1.6\mu m^{-1} \leq x < 3.69\mu m^{-1},$$
$$A_\lambda/A_V(x) = 1.3468 + 0.0087x, \quad 3.69\mu m^{-1} \leq x \leq 8\mu m^{-1}.$$

The analytic fit is shown in Fig. 6 after conversion to $\frac{E(\lambda-V)}{E(B-V)}$ using $R_V = 4.15$. This R_V value is an average of the optical/UV and the far UV values derived following CCM89 from our radio-loud reddening curves (see section 2.4).

REFERENCES

Antonucci, R. R. J. 1993, ARA&A, 31, 473

Antonucci R. R. J. 2002, in Astrophysical Spectropolarimetry, eds. J. Trujillo-Bueno, F. Moreno-Insertis, & F. Sanchez (Cambridge: Cambridge Univ. Press), p. 151.

Antonucci R. R. J. et al. 1996, ApJ, 472, 502

Avni, Y. & Tananbaum, H. 1982, ApJ, 262, L17

Baker, J. C., et al. 1997, MNRAS 286, 23

Baker, J. C., & Hunstead, R. W. 1995, ApJ, 452, L95

———— 1996a, ApJ, 461, L59 (Erratum)

———— 1996b, ApJ, 468, L131 (Erratum)

Baker, J. C., Hunstead, R.W., Athreya, R. M., Barthel, P. D., de Silva, E., Lehnert, M. D., & Saunders, R. D. E. 2002, ApJ, 568, 592

Barr, P. 1982, in ESA 3rd European IUE Conf., p. 559

Bechtold, J., Shields, J., Rieke, M., Ji, P., Scott J., Kuhn, O., Elvis, M., & Elston, R. 1997, in ASP Conf. Ser. 113, Emission Lines in Active Galaxies: New Methods and

Techniques, ed. B. M. Peterson, F.-Z. Cheng, & A. S. Wilson (San Francisco: ASP), 123

Bohren C. F. & Hufman D. R., "Absorption and Scattering of light by small particles" (New York: Wiley & Sons)

Brinkman, W., Yuan, W, & Siebert, J 1997, A&A, 319, 413

Burstein, D., & Heiles, C. 1982 AJ, 87, 1165

Calzetti, D., Kinney, A. L., & Storchi-Bergmann, T. 1994, ApJ, 429, 582.

Cardelli, J. A., Clayton G. C., & Mathis, J. S. 1989, ApJ, 345, 245 (CCM89)

Cheng, F. H., Gaskell, C. M., & Koratkar, A. P. 1991, ApJ, 370, 487

Clavel, J., Schulz, B., Altieri, B., Barr, P., Claes, P., Heras, A., Leech, K., Metcalfe, L., & Salama, A. 2000, A&A, 357, 839

Clavel, J., Wamsteker, W., Glass, I. S., 1989, ApJ, 337, 236

Chang, C. A., Schiano, A. V. R., & Wolfe, A. M. 1987, ApJ, 322, 180

Collier, S. J. 2001, MNRAS, 325, 1527

Collier, S. J., et al. 1998, ApJ, 500, 162

Collier, S. J., et al. 2001, ApJ, 561, 146

Crenshaw, D. M., Kraemer, S. B., Bruhweiler, F. C., & Ruiz, J. R. 2001, ApJ, 555, 663

Crenshaw, D. M., Kraemer, S. B., Turner, T. J., Collier, S., Peterson, B. M., Brandt, W. N., Clavel, J., George, I. M., Horne, K., Kriss, G. A., Mathur, S., Netzer, H., Pogge, R. W., Pounds, K. A., Romano, P., Shemmer, O., & Wamsteker, W. 2002, ApJ, 566, 187

De Zotti, G., & Gaskell, C. M. 1985, A&A, 147, 1

Draine, B. T. & Salpeter, E. E. 1979, ApJ, 231, 77

Dultzin-Hacyan, D., and Ruano, C. 1996, A&A305, 719

Fischera, Jg., Tuffs, R. J., Völk, H. J. 2002, A&A, 395, 189

Fizpatrick, E. L., & Massa, D. 1988, ApJ, 328, 734

Francis, P. J., Hewett, P. C., Foltz, C. B., Chaffee, F. H. 1992, ApJ, 398, 476

Gaskell, C. M., Doroshenko, V. T., Klimek, E. S., Crowley, K. A., George, T. A., Grove, R., Hedrick, C. H., Hiller, M. E., Peterson, B. W., & Poulsen, M. A. et al., 2004, in preparation

Gaskell, C. M. & Klimek, E. S. 2003, A&ApT, 23, 22, 661.

Goodrich, R. W. 1989, ApJ, 340, 190

Goosmann, R. W. 2002, Diplomarbeit thesis, Univ. Hamburg

Gordon, K. D., Hanson, M. M., Clayton, G. C., Rieke, G. H., & Misselt, K. A. 1999, ApJ, 519, 165

Gordon, K. D., & Clayton, G. C. 1998, ApJ, 500, 816

Grandi, S. A. 1983, ApJ, 268, 591

Grossan, B., Remillard, R. A., Bradt, H. V., Brissenden, R. J., Ohashi, T., & Sakao, T. 1996, ApJ, 457, 199

Hall, P. S. et al., 2002, ApJS, 141, 267

Imanishi, M. 2001, AJ, 121, 1927

Kembhavi, A. 1997, MNRAS, 264, 683

Korista, K. T. & Goad, M. R. 2001, ApJ, 553, 695

Kriss, G. A., Peterson, B. M., Crenshaw, D. M., Zheng, W. 2000, 535, 58

Kriss, G. A. & Canizares, C. R. 1985, ApJ, 297, 177

Krolik, J. H. & Begelman, M. C. 1988, ApJ, 329, 702

Laor, A., Draine, B. T, 1993, ApJ, 402, 441

Maccacaro, T., Perola, G. C., & Elvis, M. 1982, ApJ, 257, 47

Maiolino, R., Marconi, A., & Oliva, E. 2001a, A&A, 365, 37

Maiolino, R., Marconi, A., Salvati, M., Risaliti, G., Severgnini, P., Oliva, E., La Franca, F., & Vanzi, L. 2001b, A&A, 365, 28

Malkan, M. A. 1984, in "X-Ray and UV Emission from Active Galactic Nuclei", Max-Planck Inst. Reports, Vol. 184, p. 121

Maoz, D., Korista, K. T., Shapovalova, A. I., Shields, J. C., Smith, P. S., Thiele, U., Wagner, R. M. 1993, ApJ, 404, 576

Martel, A. R. 1998, ApJ, 508, 657

Mathis, J. S. 1990, ARA&A, 28, 37

Mathis, J. S., Rumpl, W., & Nordsiek, K. H. 1977, ApJ, 217, 425 (MRN)

McKee C. F., & Petrosian V. 1974, ApJ, 189, 17

Miller, J. S., Goodrich, R., & Mathews, W. G. 1991, ApJ, 378, 47.

Misselt, K. A., Clayton, G. C., & Gordon, K. D. 1999, ApJ, 515, 128

Mushotzky, R. F. & Wandel, A. 1989, ApJ, 339, 674

Netzer H. 1985, ApJ, 289, 451

Netzer H., & Davidson K. 1979, MNRAS, 187, 871

Netzer H., Brotherton M. S., Wills B. J., Han M. S., Wills D., Baldwin J. A., Ferland G. J., & Browne, I. W. A. 1995, ApJ, 448, 27

Ogle, P. M., Brookings, T., Canizares, C. R., Lee, J. C., & Marshall, H. L. 2003, A&A, 402, 849.

Oknyanskij, V. L., Horne, K., Lyuty, V. M., Sadakane, K., Honda, S., & Tanabe, S.in Active Galactic Nuclei, from Central Engine to Host Galaxy, eds. S. Collin, F. Combes and I. Shlosman. ASP Conf. Ser, Vol. 290, p. 119

Perola, C. et al. 1982, MNRAS, 200, 293

Pitman K. M., Clayton G. C., & Gordon K. D. 2000, PASP, 112, 537

Reichert, G. A., Mason, K. O., Bowyer, S. & Thorstensen, J. R. 1982, ApJ, 260, 437

Reichert, G. A., Mushotzky, R. F., Holt, S. S., & Petre, R. 1985, ApJ, 296, 69

Rieke G. H., & Lebofsky M. J. 1985, ApJ, 288, 618

Richards, G. T. et al., 2003, AJ, 126, 1131

Risaliti, G., Elvis, M., & Nicastro, F. 2002, ApJ, 571, 234

Sambruna, R. M., Eracleous, M., & Mushotzky, R. F. 199, ApJ, 526, 60

Schmitt, H. R., Kinney, A. L., Calzetti, D., Storchi-Bergmann, T. 1997, AJ, 114, 592

Shastri, P. 1991, MNRAS, 249, 640

Siebenmorgen, R., Krgel, E., & Spoon, H. W. W. 2004, A&A, 414, 123

Snedden, S. A. & Gaskell, C. M. 2004, ApJ, submitted.

Wandel, A. & Petrosian, V. 1988, ApJ, 329, L11

Ward M. J., Elvis M., Fabbiano G., Carleton N. P., Willner S. P., & Lawrence A. 1987, ApJ, 315, 74

Ward, M. J. & Morris, S. L. 1984, MNRAS, 207, 867

Weingartner J. C., & Draine B. T. 2001, ApJ, 548, 296

Wills, B. J. 1999, in Quasars and Cosmology, ASP Conference Series 162, ed. G. J. Ferland & J. A. Baldwin. (San Francisco: Astron. Soc. Pacific), p. 101

Wills, B. J., Shang, Z.-H, & Yuan, J. M. 2000, New Ast. Rev. 44, 511

Zamorani, G., Henry, J. P., Maccacaro, T., Tananbaum, H., Soltan, A., Avni, Y., Liebert, J., Stocke, J., Strittmatter, P. A., Weymann, R. J., Smith, M. G., & Condon, J. J. 1982, ApJ, 245, 357

Table 1. Estimates of the Ratio of Total to Selective Extinction

Data sets	IR-extrap.	opt./near-UV	far-UV
$\Re < 0.1$ to $\Re \geqslant 1$	5.30 ± 0.15	5.55 ± 0.15	5.40 ± 0.20
CSS to $0.1 \leqslant \Re < 1$	4.95 ± 0.15	4.95 ± 0.15	4.80 ± 0.15
LBQS to $\Re \geqslant 1$	3.70 ± 0.25	3.80 ± 0.20	3.20 ± 0.20

Table 2. Effect of Host Galaxy Contamination on Inferred Reddening

AGN/Host	E(B-V)$_{opt}$	E(B-V)$_{UV-opt}$
10	0.02	0.04
5	0.04	0.07
1	0.12	0.31
0.5	0.17	0.54
0.1	0.25	1.50

Table 3. AGN Extinction at Major Emission Lines and Wavebands

Line	λ [Å]	A_λ/A_V
O I	8446	0.579
H α	6563	0.826
He I	5876	0.932
V band	5500	0.994
H β	4861	1.103
He II	4686	1.133
B band	4400	1.182
He I	4471	1.170
H γ	4340	1.193
Mg II	2798	1.377
C II]	2326	1.384
C III]	1909	1.392
He II	1640	1.400
C IV	1549	1.403
O IV]/Si IV	1400	1.409
O I	1304	1.414
N V	1240	1.417
Ly α	1216	1.418
O IV	1034	1.431

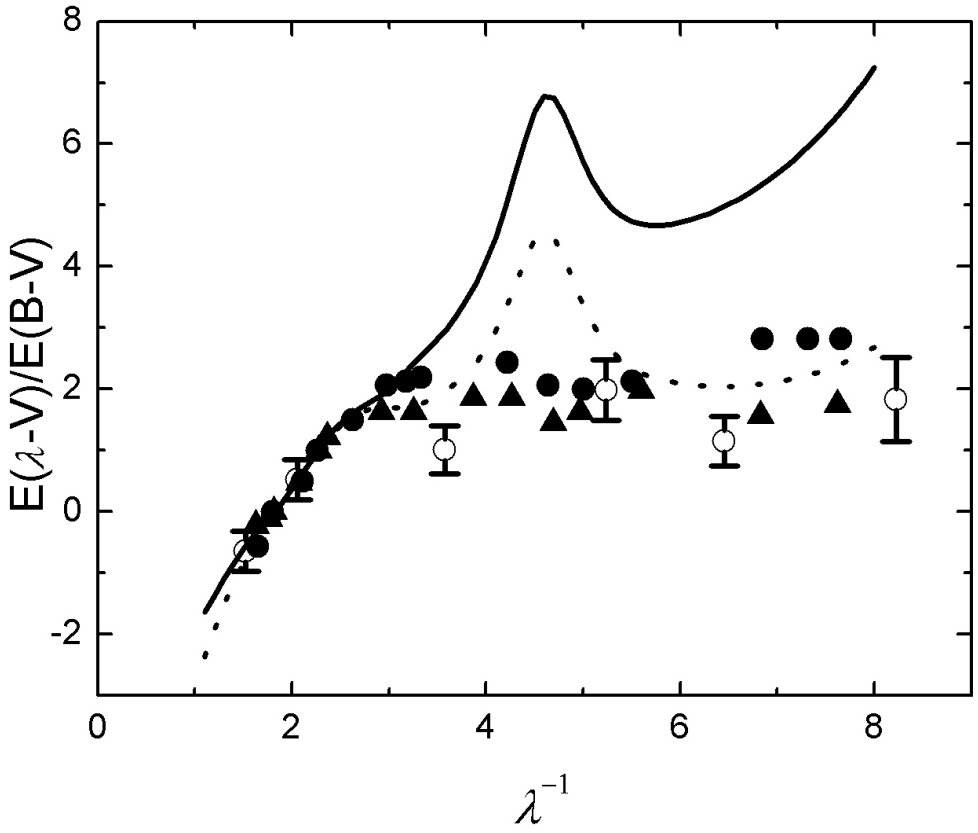

Fig. 1.— Reddening curves (in magnitudes vs. $\mu\mathrm{m}^{-1}$) based on the Baker & Hunstead (1995, 1996) data subsets for composite spectra. Filled triangles are from comparing $\Re \geqslant 1$ with $\Re \leqslant 0.1$ and filled circles are from comparing $0.1 \leqslant \Re < 1$ with CSS. The open circles represent average BLR extinction values between face-on ($\Re \geqslant 1$) and edge-on ($\Re < 0.1$, CSS) objects. Theoretical reddening curves derived from CCM89 for $R_V = 5.3$ and $R_V = 3.1$ are shown as dashed and solid curves respectively.

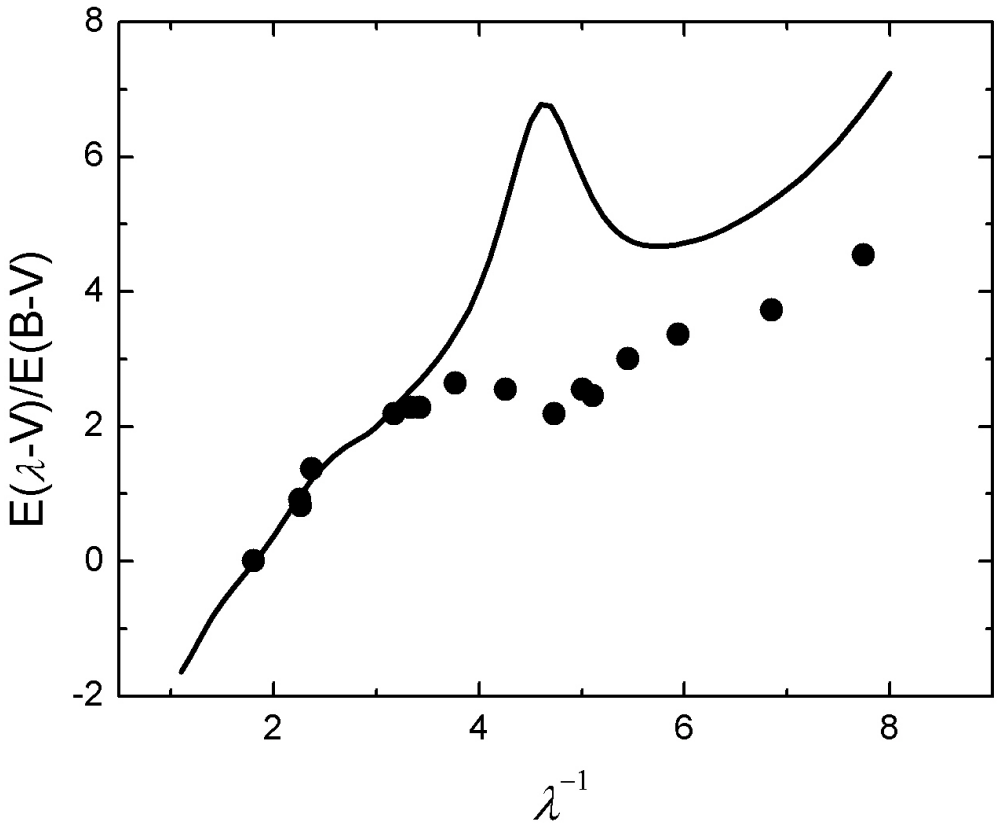

Fig. 2.— Reddening curve (units as in Fig. 1) based on the Baker & Hunstead data for the composite spectrum $\Re \geqslant 1$ compared to the LBQS sample (circles). Computed reddening curve derived from CCM89 for $R_V = 3.1$ (solid curve).

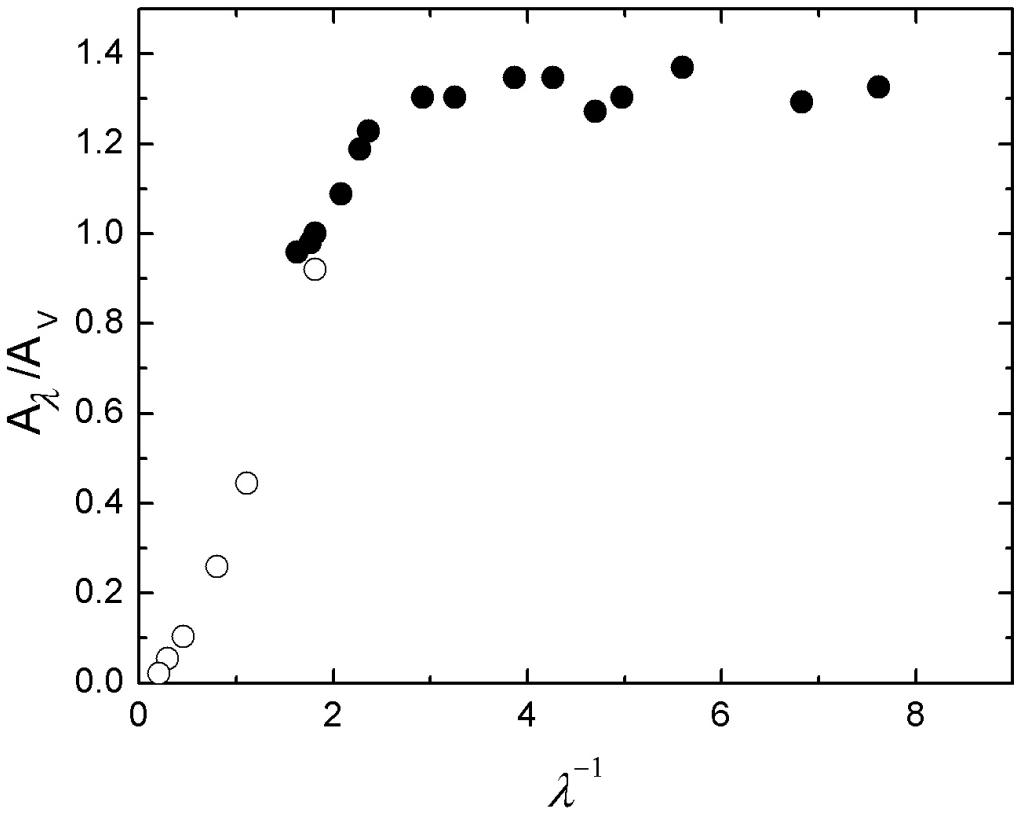

Fig. 3.— Optical and UV reddening curve, in magnitudes as a function vs. inverse wavelength (μm^{-1}), between the composite spectra $0.1 \leqslant \Re < 1$ and CSS (filled circles) with an extrapolation into the IR based on Rieke & Lebofsky (open circles).

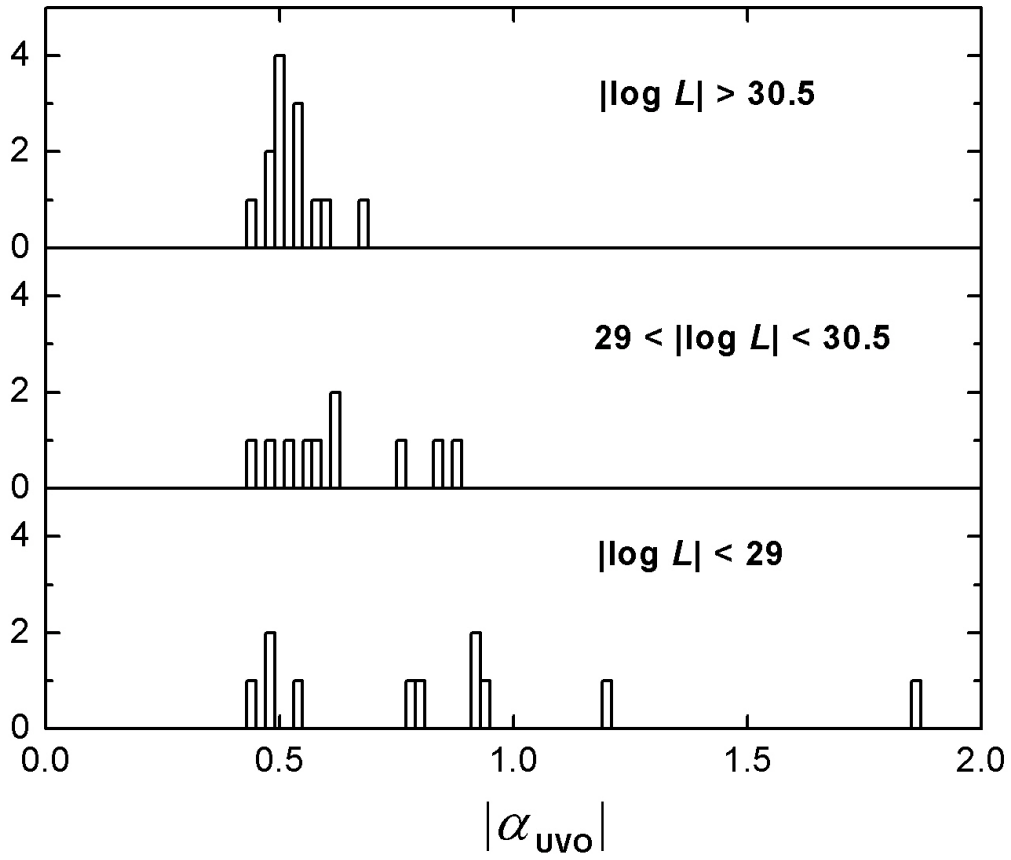

Fig. 4.— Number distribution of α_{UVO} for AGNs in three different monochromatic optical luminosity (L_{4200}) ranges, $|logL| > 30.5$ (a), $29 < |logL| < 30.5$ (b) and $|logL| < 29$ (c)

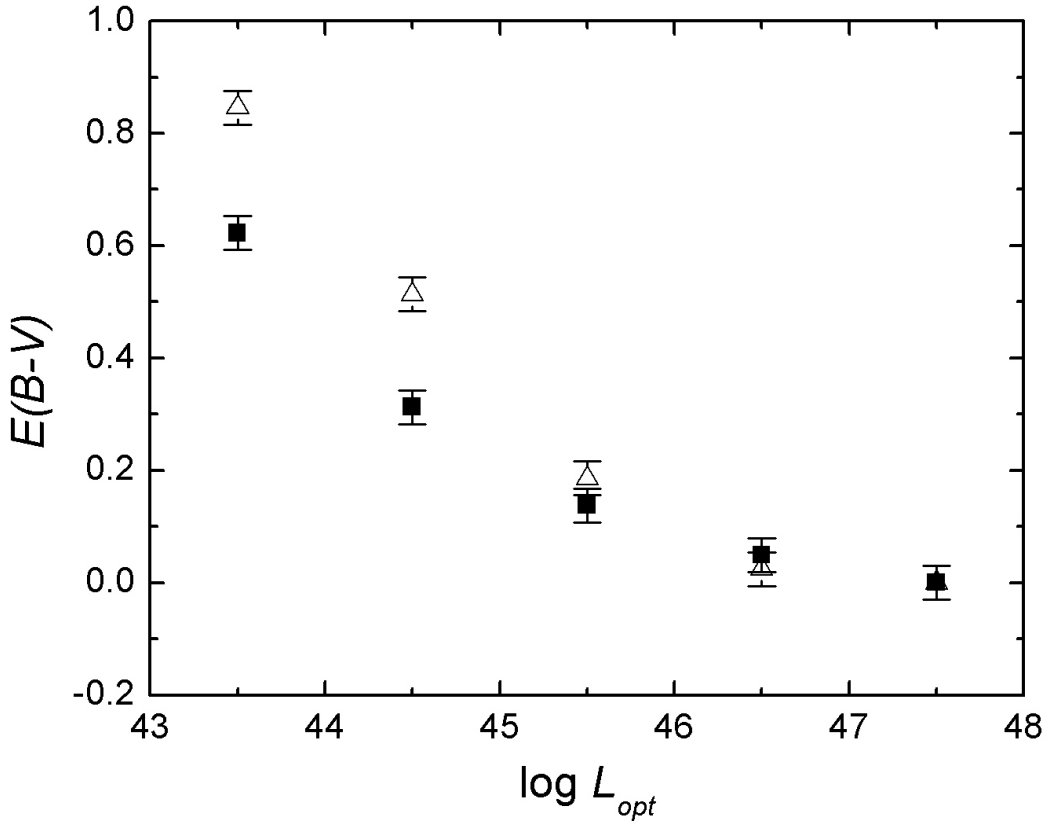

Fig. 5.— The mean reddenings, (E(B-V)), inferred using the extinction curve in Fig. 1, plotted as a function of observed optical luminosity of the AGNs (in ergs s^{-1}). The solid squares are reddenings derived from the λ1600 to λ4200 spectral index; the open triangles are the reddenings derived from the λ4200 to λ7000 spectral index. The trends are similar using the optical and UV diagnostics.

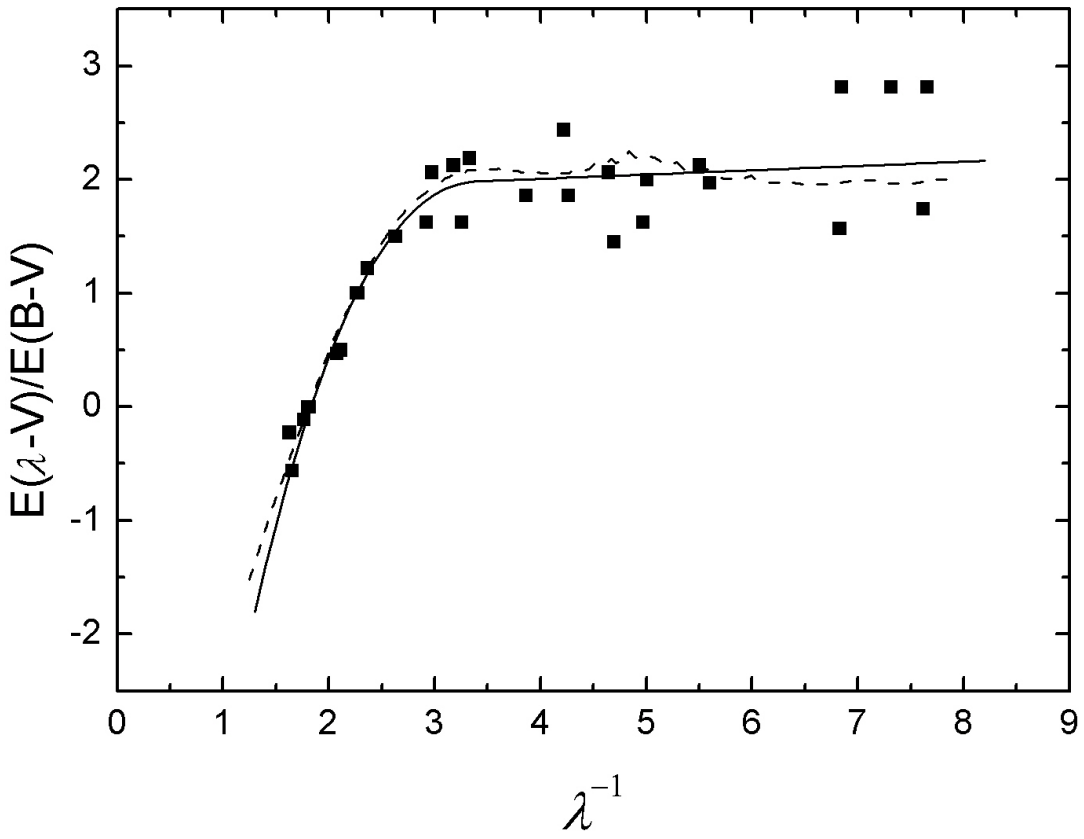

Fig. 6.— AGN extinction curves (squares) plotted together with a model curve derived from Mie theory computations (dotted line, see section 6.2) and the analytical fit given in the Appendix (solid line)